A Petrologic and Petrochemical Investigation of Magmatic Phases in the Powderhorn Carbonatite Complex, Gunnison, Colorado

Alexander Marr*

*Department of Geosciences, 1000 Rim Drive, Fort Lewis College, Durango, CO 81301

ABSTRACT

The Powderhorn Complex is composed of carbonatite and several varieties of alkaline ultramafic rocks that include ijolite, uncompahgrite, pyroxenite, and nepheline syenite. Sr and Nd isotope data and bulk rock geochemistry collected in this study were combined with data from previous studies to gain further insight into the magma source and history of the rocks in this complex.

$^{87}Sr/^{86}$ Sr ratios range from 0.703106 to 0.703632 and εNd values from Premo and Lowers (2013) range from 1.4-3.1. The bulk-rock isotope data, when combined with whole-rock geochemistry, indicate that parent magmas for these rocks came from a similar mantle source with minor heterogeneity or that there was minor crustal contamination during emplacement. All the rocks in the complex are LREEs (light rare earth elements) enriched with concentrations from 100 times more than compared to primitive mantle and chondrite. On a variety of discrimination plots, the data for the different rocks define distinct fields, and only the trends for the pyroxenite samples are consistent with crystal fractionation. There is no convincing evidence that fractionation of the pyroxenite generated the other lithologies, contrary to previous investigations. This is also supported by the distinct mineralogic assemblages for each rock type which are not easily explained by fractional crystallization.

The Powderhorn Complex was formed by the generation of different magma compositions from a similar mantle source. Minor variations in source composition or different degrees of partial melting could explain the different compositions of the various rocks in the complex. It is also possible that these rocks were formed through a combination of these processes.

ACKNOWLEDGEMENTS

Thank you so much to my advisors, David Gonzales and Kim Hannula. Thank you David for suggesting the idea for this thesis, taking me to the field to collect samples, providing articles, arranging and sending thin sections, isotope and geochemical samples, arranging funding from Newmont Partnership Funding, help interpret the data, and organizing and proofreading this thesis. Thank you Kim for sending thin section samples, arrange funding from the Peter Mesard Undergraduate Funding, helping me organize and proofread this report, giving me encouragement to get through, and answering my 1000 questions.

I would also like to thank Emily Verplanck of Colorado University Boulder and Dr. Elizabeth Griffith of the Ohio State University for the isotope analysis and data.

Thank you very much Dr. Allen Stork of Western State University for assistance in the field, providing GIS information and the nepheline syenite sample, and information about contamination at the complex.

This project would not have been possible with Newmont Partnership Funding and the Peter Mesard Undergraduate Research Funding providing funds for the thin sections, and isotopic and geochemical analyses.

Big thanks to Andrea Kirkpatrick for helping download IgPet which was used to create the geochemical and isotope plots, and Tim Birchard and Jenny Mason for proofreading this report.

Finally, I would love to give huge thanks to my mom and dad for being supportive and caring throughout my life, and giving me the confidence to get through this thesis. Without their support and love, I would not be here.

INTRODUCTION

The Powderhorn Carbonatite Complex (also known as the Iron Hill Carbonatite Complex; for this project, we'll be calling it Powderhorn) is a suite of mantle-derived magmatic rocks exposed about 35 km southwest of Gunnison, Colorado (Fig. 1). Previous mapping projects and investigations revealed there are five different rock clans in the complex. From oldest to youngest, these are: pyroxenite, uncompaghrite, ijolite, nepheline syenite, and carbonatite. The rocks serve as resources for REEs, thorium, niobium, titanium, iron, uranium, and vanadium deposits (Armbrustmacher, 1981; Erickson, 2014; Cappa, 1998).

Despite the results of earlier studies at the Powderhorn complex, there are still some critical questions about these rocks that are important in understanding their origin and history. According to Erickson (2014), Sr and Nd isotope work would help support earlier propositions that the earliest rock clans in the complex originated from the partial melting of a primitive mantle source. The isotope data will help define a potential mantle reservoir. In this investigation, detailed petrologic and petrochemical studies were done on all major rock types in the Powderhorn complex. These data are combined with $^{87}Sr/^{88}Sr$ and $^{143}Nd/^{144}Nd$ isotope data to define a potential mantle reservoir and determine the origin and magmatic relationships of the rocks during their formation.

Geological Setting

The Powderhorn complex is located 35 miles southwest of Gunnison, and just outside of the hamlet of Powderhorn in Gunnison County, Colorado. The complex is exposed over an area of around 31 square kilometers (about 12 square miles). The complex consists of five different clans from oldest to youngest: pyroxenite, uncompaghrite, ijolite, nepheline syenite, and carbonatite. The oldest unit, the pyroxenite, has been dated multiple times: 570 Ma from K-Ar on

biotite and hornblende and Rb-Sr whole rock (Olson et al., 1977), 603 Ma from Pb/Pb whole rock (Premo and Lowers, 2013), and 617 Ma from Rb-Sr whole rock (Premo and Lower, 2013).

The core of the complex consists of a carbonatite stock that is mantled by four different clans of rocks dominated by silicate minerals (Fig. 1). From oldest to youngest, they are pyroxenite, uncompaghrite, ijolite, nepheline syenite, and carbonatite. The pyroxenite covers about 70% of exposed bedrock at Powderhorn Carbonatite Complex, has sharp contacts with the surrounding host rocks, and occupies a topographic low on the west side. The uncompaghrite crops out in the southern part of Powderhorn. The ijolite intrudes the pyroxenite and uncompaghrite in the southeastern portion of the complex. The nepheline syenite is exposed in the eastern portion of the complex and occurs as small stocks and dikes in the Proterozoic granite, fenite, and pyroxenite. Finally, the carbonatite is the prominent rock of Big and Little Iron Hills and was emplaced as a stock. Numerous carbonatite dikes crosscut pyroxenite, Proterozoic granite, and fenitized rock (Cappa, 1998).

The Powderhorn Complex is surrounded by Proterozoic metamorphosed sedimentary and volcanic rocks (Erickson, 2014). The complex is covered by Paleozoic and Mesozoic sedimentary units in some areas (Larsen, 1942; Hedlund and Olson, 1981), and is capped by Oligocene volcanic rocks to the northwest (Cappa, 1998). At depth the complex is thought to be funnel shaped according to drill data (Temple and Grogan, 1965). The northwest-southeast trending Laramide-era Cimarron Fault (Hedlund and Olson, 1981) bisects the complex and exposes deeper structure of the alkaline component northeast of the fault zone (Armbrustmacher, 1981).

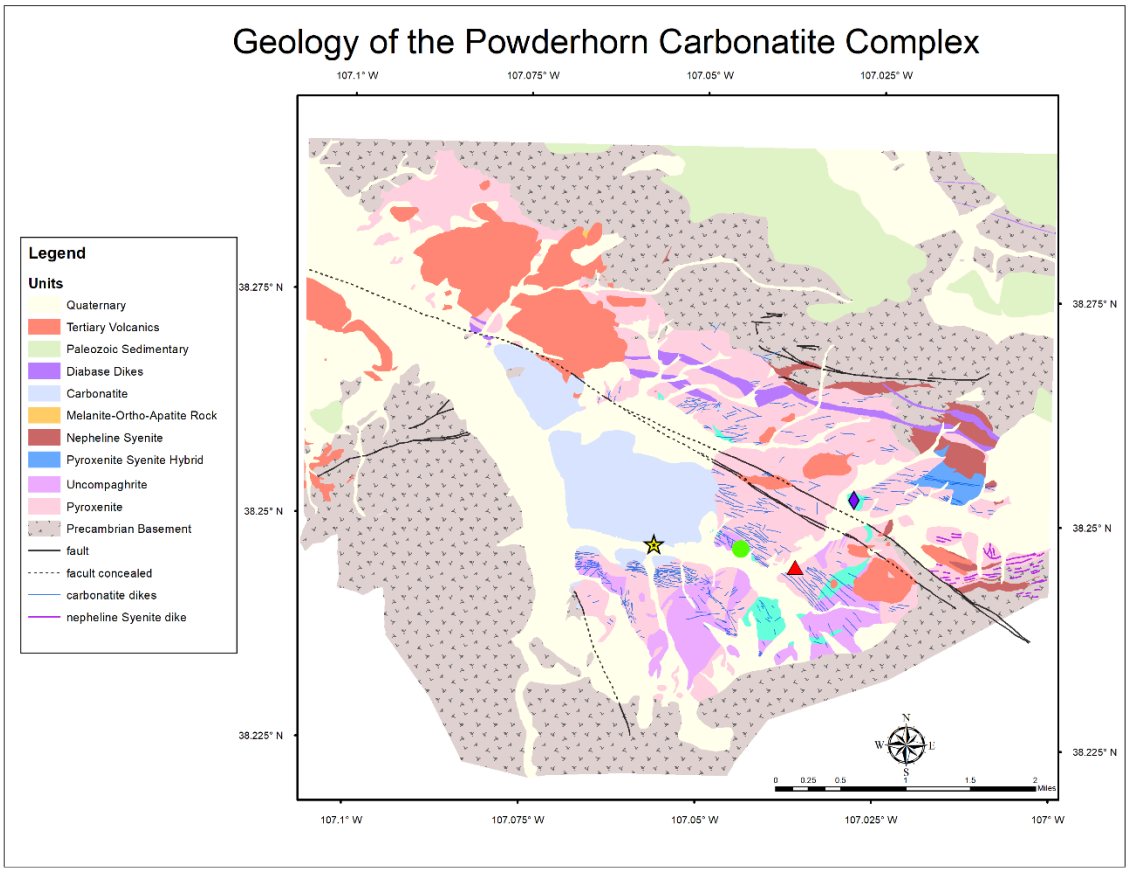

Figure 1: The geological map of the Powderhorn Carbonatite Complex. The following symbols are where the individual rock type samples are collected: gold star, carbonatite; green circle, uncompahgrite, red triangle, pyroxenite; and purple diamond, ijolite.

The Powderhorn carbonatite complex is part of a series of other carbonatite, syenite, and mafic rocks that are scattered through southern Colorado and northern New Mexico, ranging in ages between 664-457 Mya (late Neoproterozoic to Ordovician), in what was then the western margins of Laurentia. These rocks formed in an extensional system in the area around this time (McMillan and McLemore, 2004). During this time, the supercontinent Rodinia was breaking apart (between 750 to 633 Mya according to Li et al. (2008)). According to Goetz and Dickerson (1985), there was an intermittently active transform zone in what is now modern day southwest North America, from the late Proterozoic into the Triassic. In these transform zones, differential movements created rift zones, and those zones that failed to become fully developed rift zones are called aulacogens. One of these aulacogens has a north-south trend extending from southern New Mexico to northern Colorado (McMillan and McLemore, 2004). Its eastern boundary is around

the New Mexico-Texas border, and the western is on the New Mexico-Arizona border (McMillan and McLemore, 2004). The Powderhorn Carbonatite is found near the northern center of this aulacogen (Figure 2)

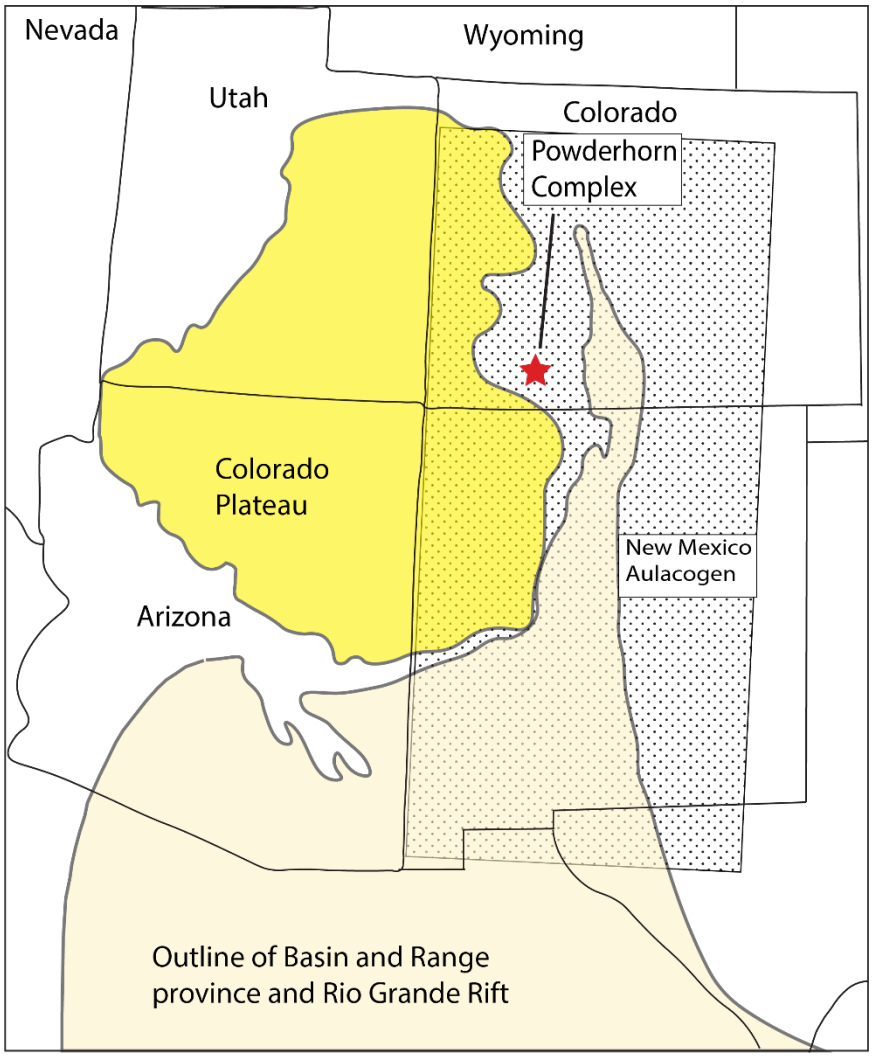

Figure 2: Map of the late Precambrian-Ordovician New Mexico Aulacogen with modern day geological provinces, and the location of the Powderhorn Complex. Modified from McMillian and McLemore (2004

Overview of Carbonatites

Carbonatites are rare types of igneous rocks characterized by distinct mineralogies and chemistries. Most of the igneous rocks exposed on Earth contain a high percentage of quartz and feldspars, but carbonatites are dominated by carbonate minerals and associated rocks have high concentrations of minerals that are low in silica. Carbonatites contain more than 50% primary carbonate minerals and less than 20% SiO_2 according to the International Union of Geological Sciences (Le-Maitre, 2002). The nomenclature of carbonatites is based on their dominant carbonate mineral and their corresponding major element geochemistry. Carbonatites that are dominated by calcite are called calcite-carbonatites or calciocarbonatites. Dolomite is the dominant mineral in dolomite-carbonatites or magnesiocarbonatites, and ankerite is the primary mineral in ferrocarbonatites (Le Maitre, 2002). The carbonatite at the Powderhorn is predominantly a ferrocarbonatite. Carbonatites are usually associated with wide ranges of alkaline rocks such as melilitolite, nephelinite, pyroxenite, syenite, and lamprophyre (Bell, 1998; Jones, 2013). There are 527 known carbonatites found throughout the world, ranging in age from Archean to Holocene. Carbonatites are dominantly found on ancient cratonic crust, shields, and crustal blocks, such as eastern Africa (Jones, et al 2013; Berger, 2009). Many carbonatite complexes are important sources of rare earth elements which are used to produce cell phones, batteries, high powered magnets and other products (Rare Earth Elements, 2016).

There are three hypotheses on how carbonatites are formed: fractionation crystallization of a syenite magma liquid, liquid immiscibility, and partial melting of carbon-dioxide rich mantle peridotite.

1. In the fractional crystallization hypothesis, the carbonatite magma is the last crystallized fraction of a syenite, carbonated nephelinite, and/or melilitite melt (Gittins, 1989; Gittins and Jago, 1998). In this process, the magmatic mineral chemistry should have continuous

primary magmatic mineral chemistry trends, with the youngest being the most enriched in trace elements, and the oldest most depleted. Crystal fractionated rocks have high concentration of incompatible elements such as REEs, which were partitioned into the melt during crystallization. This results in the youngest, last crystallized rocks having a high concentration of incompatible elements, and explains why carbonatite complexes are rich in REEs. While this genesis explains the temporal and spatial association of carbonatites and alkaline rocks, it does not explain why carbonatite complexes don't have an intermediate composition between the carbonatites and alkaline rocks (Erickson, 2014).

2. For immiscibility model hypothesis, the carbonate melt fractionates from a carbonated silicate melt (Koster van Groos and Wyllie, 1963; Kjarsgaard and Hamilton, 1989). Before immiscibility, both magmas started from the same homogeneous magma, and were divided when a solvus was reached. After immiscibility, the magmas were still in equilibrium with each other. This hypothesis is supported by displaying similar isotopic characteristics between the carbonatite and alkaline rocks (Winter, 2010; Halama et al, 2004; Bell 1998). Harmer and Gittins (1998) showed that liquid immiscibility between carbonate and silicate melt is only relevant at low pressure crustal condition, and does not occur in mantle melts or pressure. This model explains why carbonatite complexes have a lack of intermediate lithologies, and similar isotopic characteristics between the carbonatites and the alkaline rocks at Powderhorn (Erickson, 2014).
3. Finally, the last hypothesis says that carbonatites are formed through partial melting of carbonate-rich peridotites from the mantle. Previous experiments showed that the partial melting of carbonate-rich peridotites at a depth of more than 70 km can produce carbonate-rich magmas (carbonatite composition ranges from dolomitic, calcic, and silicic) with REE

enrichment (Wyllie and Huang, 1975; Wyllie and Lee, 1998; Brey et al, 2008). Partial melting of mantle lherzolite was shown to produce dolomitic carbonatite magmas (Wyllie and Huang, 1975; Wyllie and Lee, 1998). According to field evidence, it is shown that calciocarbonatites occur in rifted regions such as the East African Rift Zone, and dolomitic carbonatites occur in old shields such as the cratons in South Africa, and the Canadian Shield (Harmer, 1999). This is explained according to experimental studies by Harmer and Gittens (1997): the partial melting of carbonated mantle peridotite creates high Mg and 6% alkali contents, yielding a dolomitic carbonate melt. As the dolomitic melt moves through the mantle and remains in equilibrium, it will be destroyed by reacting with the lherzolite and harzburgite walls. But if the melt quickly rises out of the mantle (rifting) before reaching equilibrium, and react with wehrlite (covering the lherzolite and harzburgite wall), the melt will become calcitic. The problem with this process is that it does not explain the genesis of the alkaline rocks, it is only used for carbonatites genesis (Brey et al, 2008).

METHODS

Whole-rock geochemical data (Appendix A) were obtained for each rock to help chemically characterize each rock sample, understand the magmatic relation of the Powderhorn carbonatite complex, and be compared to other carbonatite complexes. Before being sent out for analysis, whole rock samples of each rock type without or with minor alteration were powdered and sent out to Activation Laboratory. The major elements were quantified through inductively coupled plasma–atomic emission spectroscopy (ICP-AES) using a lithium-metaborate/tetraborate fusion. The trace elements are determined through inductively coupled plasma–mass spectrometry (ICP-MS) using a sodium peroxide fusion (summarized in Gonzales and Lake, 2016).

Samples for major elements analysis are prepared and analyzed in a batch system. Before sample fusion, the samples were heated at a temperature of 1050 °C for 2 hours to allow volatiles such as H_2O^+, CO_2, and S to evaporate. The samples are then mixed with flux of lithium metaborate and lithium tetraborate, fused in an induction furnace. The molten melt is put into a solution of 5% nitric acid, and an internal standard and were mixed until the sample is completely dissolved. The samples were then analyzed for major oxides and selected trace elements (Code 4B) in a Thermo Jarrell-Ash ENVIRO II ICP or a Varian Vista 735 ICP. The calibration is performed using prepared USGS and CANMET certified reference materials. One of the seven standards is used for every group of ten samples during the analysis (Gonzales and Lake, 2016).

Samples for trace element analysis were fused under Code 4B2, diluted and analyzed by the Perkin Elmer Sciex ELAN 6000, 6100, or 9000 ICP/MS. Three blanks and five controls were analyzed per group of samples. Duplication after every 15 samples were fused and analyzed. The instrument was calibrated after every 40 samples. Repetitious measurements of standards indicated that analytical errors are at 95% (Gonzales and Lake, 2016).

Originally, bulk samples from each clan were analyzed for their initial Sr and Nd isotopes set to an age of 600 Ma at Colorado University Boulder. The Sr analysis was completed before the Nd. During the Nd analysis, the TIMS had a malfunction, preventing the complete analysis of the Nd isotopes. In response to this obstacle, the initial Nd from Premo and Lowers (2013) was incorporated into this project and compared to our Sr isotopes.

This assessment was conducted by using Thermal Ionization Mass Spectroscopy (TIMS). A Finnagan-MAT 6-collector solid source mass spectrometer was used to perform isotopic analysis. Before beginning the analysis, the Sr and Nd were separated by having their respected

rock crushed to coarse-medium sized grains and dissolved by hydrofluoric and perchloric acids. The isotopes are then separated by using the resins: Eichrom Sr, TRU, and Ln (Farmer et al, 1991).

RESULTS

Petrology

Table 1: SITE DESCRIPTION OF EACH ROCK TYPE COLLECTED IN THE FIELD

Sample Name	Rock Type	Latitude (N)	Longitude (E)	Site Description
AM-Iron Hill-Uncom-1	Uncompaghrite	38.24689	107.04417	Outcrop exposed on hillside on north side of Beaver Creek, and County Road 27B.
AM-Iron Hill-Ijo-1	Ijolite	38.25259	107.02827	Sub-outcrop buried underneath soil on top of a knoll on the north side of Beaver Creek and County Road 27B.
AM-Iron Hill-Pyro-4	Pyroxenite	38.24498	107.03643	Outcrop along the east side of County Road 27C
AM-Iron Hill-Carb-1	Carbonatite	38.24722	107.05647	Sub-outcrop at the base of Iron Hill on the north side of Beaver Creek and County Road 27B.
Refer to Figure 1 for the geological map for location of rock types				

Table 2: PETROLOGICAL SUMMARY OF ROCK TYPES IN POWDERHORN

Rock Type	Magmatic Minerals	Post-Magmatic/ Hydrothermal Minerals	Alteration Minerals	Texture Description
Pyroxenite	Apatite, Augite, Biotite, Garnet, Opaque minerals Perovskite	Aegirine, Carbonate minerals	Chlorite, Fe-Ti Oxides	Large poikilitic augite crystals, 0.6-30 cm in maximum dimension, with smaller poikilitic biotite, opaque minerals, perovskite crystals, and garnet and apatite guests, 0.0012-3.75 mm.
Uncompaghrite	Apatite, Augite, Perovskite, Garnet, Melilite, Opaque minerals Perovskite	Carbonate minerals	Chlorite, Fe-Ti Oxides	Large crystals of garnet, opaque, perovskite, and augite 0.006-27 mm, surrounded by groundmass of smaller garnet, augite, and melilite, 0.006-0.9
Ijolite	Apatite, Augite, Biotite, Nepheline, Opaque minerals, Plagioclase, Perovskites,	Carbonate minerals, Amphibole, Quartz	Chlorite, Fe-Ti Oxides, Nepheline Alteration	Poikilitic biotite, and augite crystals, 0.3-9.5 mm, surrounds apatite, and perovskite guests, 0.12-4.5 mm, and is surrounded by nepheline groundmass.
Nepheline Syenite	Augite-Aegerine, Microcline, Opaque mineral, Titanite	Carbonate mineral	Fe-Ti Oxides	Large crystals of perthitic microcline, 0.2-6.0 mm, with interstitials of augite-aegerine, titanite, nepheline, and opaques, 0.04-1.75 mm

Carbonatite	Carbonate minerals, Orthoclase, Opaque minerals	Carbonate minerals, Opaque minerals	Fe-Ti Oxides	Large oikocryst crystals of carbonate minerals, 4.5 mm, with interstitials and guests of smaller carbonate minerals, orthoclase, and opaque minerals, 0.0012-3.25 mm. In some parts of this unit, heavy phlogopization has been observed.

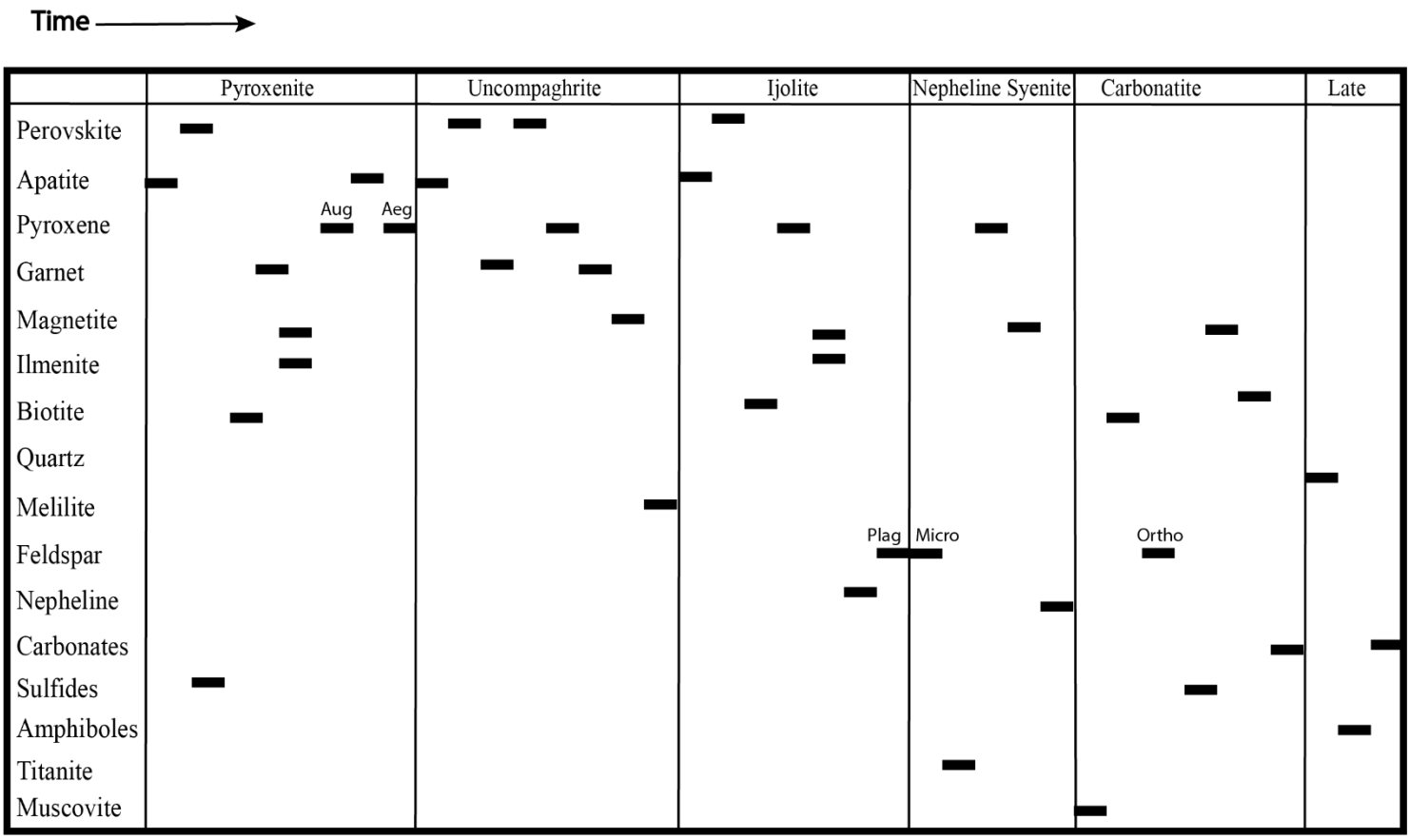

Figure 3: The petrogenesis of each mineral in their respected rock suite. All the magnetite, ilmenite, and sulfides values came from Erickson (2014). Aug, augite; Aeg, aegirine' Plag, Plagioclase; Micro, Microcline; Ortho, Orthoclase.

Pyroxenite:

The pyroxenite suite surrounds the Iron Hill carbonatite stock from the northwest to the south (Figure 1). The pyroxenite unit in this project was collected to the southeast of the carbonatite stock (Table 1). There is mineralogical variability within the pyroxenite suite: 1) coarse-grained biotite and magnetite-rich; 2) perovskite and apatite-rich; and 3) and melanite garnet-rich. These subunits were described and studied in the past by Olson and Wallace (1956); Armbrustmacher (1981); Olson and Hedlund (1981); and Van Gosen and Lowers (2007).

For this project, the coarse-grained biotite and magnetite-rich member was the only subunit sampled.There are two members in this unit, a fine-grained member and a coarse-grained member. Both members have a black to dark grey color scattered with white speckles. The fine-grained member has roughly equal size grains of pyroxene, biotite, and apatite averaging 0.3 mm. Bands of iron oxide cut through the unit. The coarse-grained member is composed of massive pyroxene crystals and large euhedral apatite crystals as long as 3 cm throughout the rock, and is spotted with biotite pods that can grow greater than 10 cm. In thin section overall, both units display a similar texture of large euhedral pyroxene oikocrysts with euhedral-subhedral apatite, biotite, garnet, perovskite, and opaque guests. Erickson (2014) reported titanite, although no titanite was found in this project. He also used SEM data to identify the opaque minerals as magnetite, ilmenite, and sulfides (mainly pyrite). Magmatic perovskite and apatite appear to have crystallized in several generations (Figure 3). Veinlets of carbonate minerals from the emplacement of the carbonatite or post-magmatic processes crosscut all magmatic minerals (Erickson, 2014). Alteration within this sample includes augite altering to chlorite, and titanium and iron rich minerals altering into titanium and iron oxides.

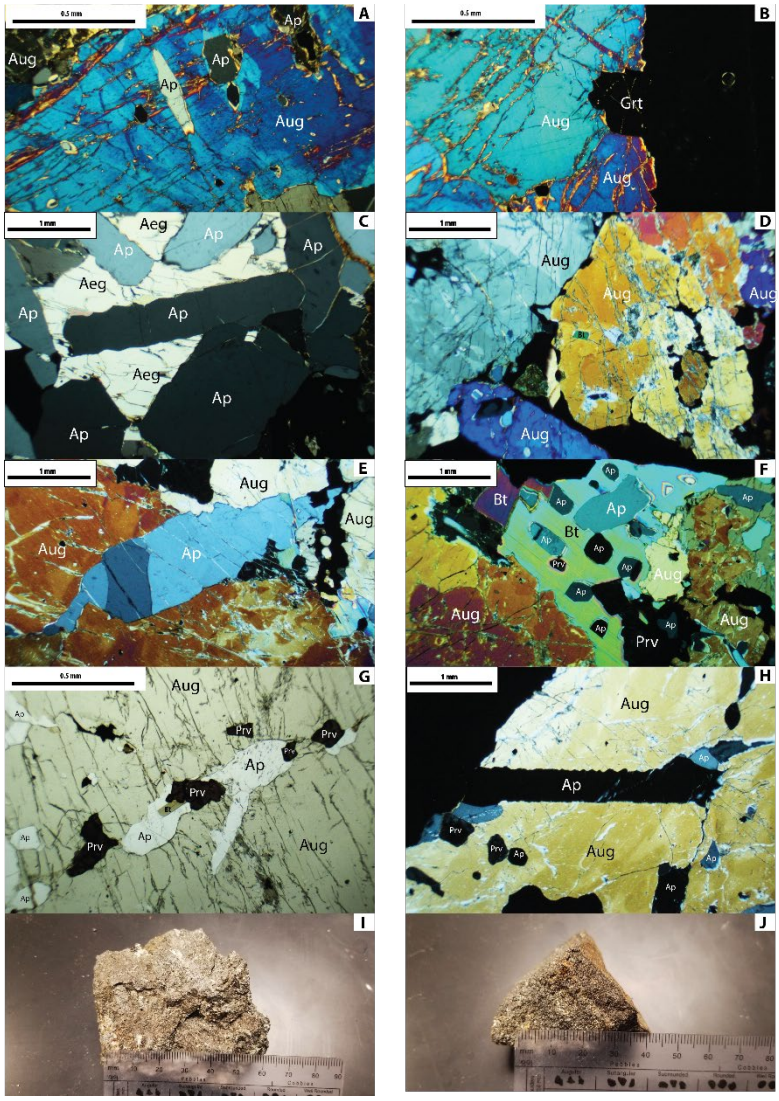

Figure 4: Microphotograph of pyroxenite taken from a transmitted light microscope. Photo A, B, E, F, G, and I are from the coarse-grained member and Photo C, D, and J are from the fine-grained member. Aeg, aegirine; Ap, apatite; Aug, augite; Bt, biotite; Grt, garnet; Prv, perovskite.

Uncompaghrite

The uncompahgrite crosscuts the pyroxenite units to the south and southwest of the carbonatite stock (Figure 1). This unit was collected to the southwest, right next to the stock (Table 1).

Uncompaghrite contains a light greenish-yellow groundmass that contain black ribbons of garnet. The groundmass has a medium grain size averaging at 3 mm and the ribbons can grow greater than 15 cm. The texture is mostly large poikilitic augite, garnet, apatite, opaque, and

perovskite crystals ranging from 0.9 mm to 27 mm with groundmass of finer crystals of augite, garnet, apatite, and melilite. The opaque mineral is mostly magnetite (Erickson, 2014). Figure 5F shows two generations of perovskite and garnet. Late hydrothermal amphiboles and carbonate veins crosscut earlier magmatic minerals. Augite has been altered to chlorite, and Ti- and Fe-rich minerals have been altered to titanium and iron oxides.

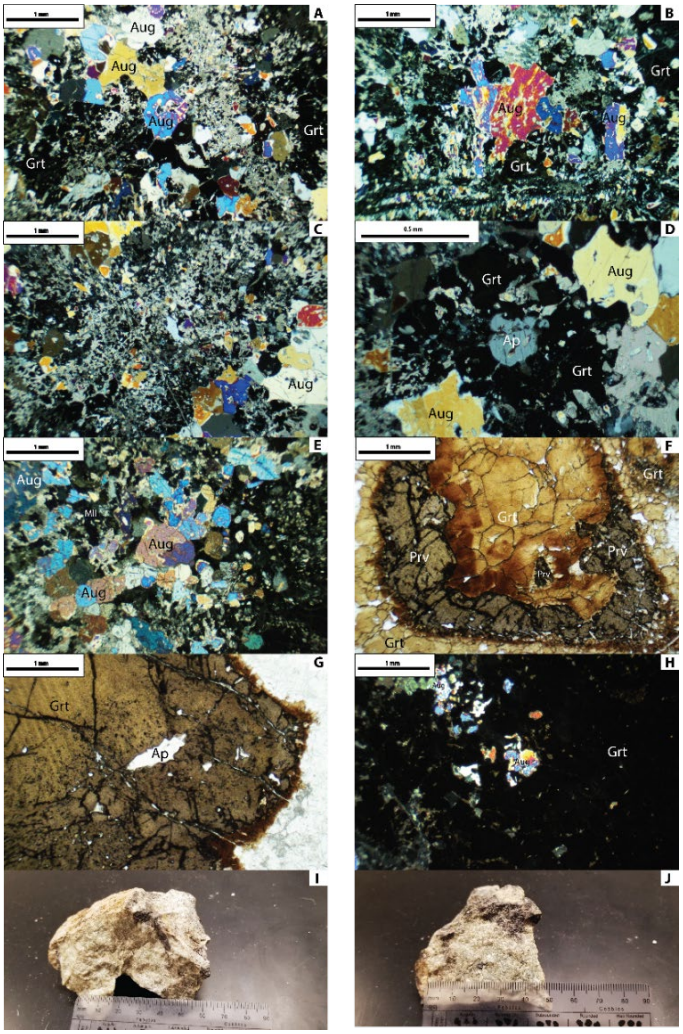

Figure 5: Microphotograph of uncompahgrite taken from a transmitted light microscope. Ap, apatite; Aug, augite; Grt, garnet; Mll, melilite; Prv, perovskite.

Ijolite

The ijolite is found to the southeast and northeast of the carbonatite stock (Figure 1). In the northeast, it crosscuts the pyroxenite, and in the southeast it crosscuts the pyroxenite and uncompahgrite. The ijolite was collected on a small knoll to the east of the stock (Table 1).

The ijolite mostly contains varying amounts of black crystals and white groundmass. The black crystals are mostly subhedral-euhedral biotite and pyroxene crystals with sizes up to 2 cm. The white groundmass is mostly composed of altered nepheline. The texture of the ijolite is composed of large biotite, opaque minerals, augite oikocrysts ranging up to 9.5 mm with apatite and augite guests, and groundmass consisting of altered nepheline, perovskite, and finer-grained biotite, augite, and apatite ranging up to 0.09 mm. The opaque minerals in this rock are magnetite and ilmenite (Erickson, 2014). Euhedral bladed plagioclase crystals with high calcium content and high interference colors (possibly from a thicker thin section) were observed (Figure 6). Orthoclase has also been reported in this rock type (Armbruscher, 1981). Hydrothermal carbonates occurred as veinlets or blebs within the groundmass (Erickson, 2014) and crosscut the magmatic crystals. Other post-magmatic minerals such as quartz veins and amphibole has been observed. Early magmatic accessory perovskite has been heavily altered to iron and titanium oxides. Augite altering to chlorite, and iron and titanium minerals to iron and titanium oxides have been observed.

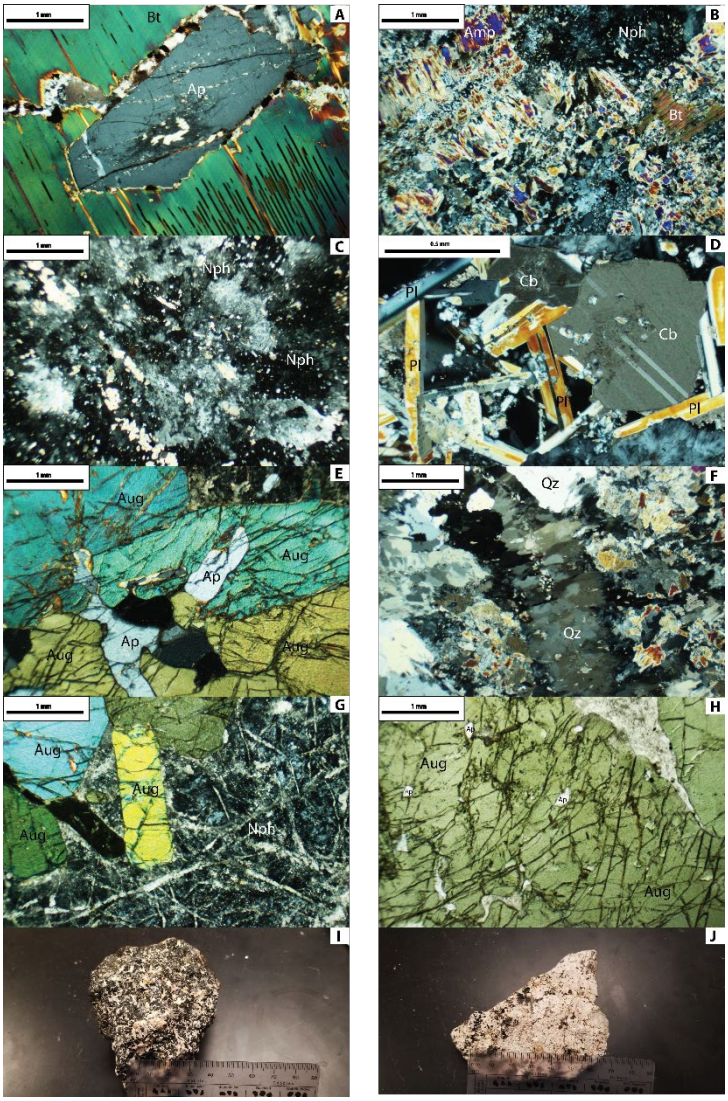

Figure 6: Microphotograph of ijolite taken from a transmitted light microscope. Amp, amphibole; Ap, apatite; Aug, augite; Bt, biotite; Cb, carbonate minerals; Nph, nepheline; Pl; plagioclase; Prv, perovskite; Qz, quartz.

Nepheline Syenite:

The nepheline syenite is located to the east and northeast of the stock, crosscutting the pyroxenite and earlier Protozoic bedrock (Figure 1). The nepheline syenite sample was not collected in the field; a sample was sent by Allen Stork from Western State University and was transformed into a thin section.

The color of the sample is light-medium grey with specks of black crystals (pyroxene). The rock is mostly made up of 5 mm potassium feldspar crystals with 3 mm pyroxene crystals. The

potassium feldspar are perthitic microcline and orthoclase. In thin section, fine-grained nepheline, aegirine-augite (Erickson, 2014) forming intimately with titanite, and opaque minerals are found scattered throughout the rock and in the interstitials of the potassium feldspars (Erickson, 2014). Opaque minerals in this rock are magnetite or ilmenite (Erickson, 2014). The rock is mostly uncontaminated by post magmatic processes, although a few microcline crystals have been crosscut by carbonate veinlets. Alteration minerals found in this rock are Fe-Ti oxides.

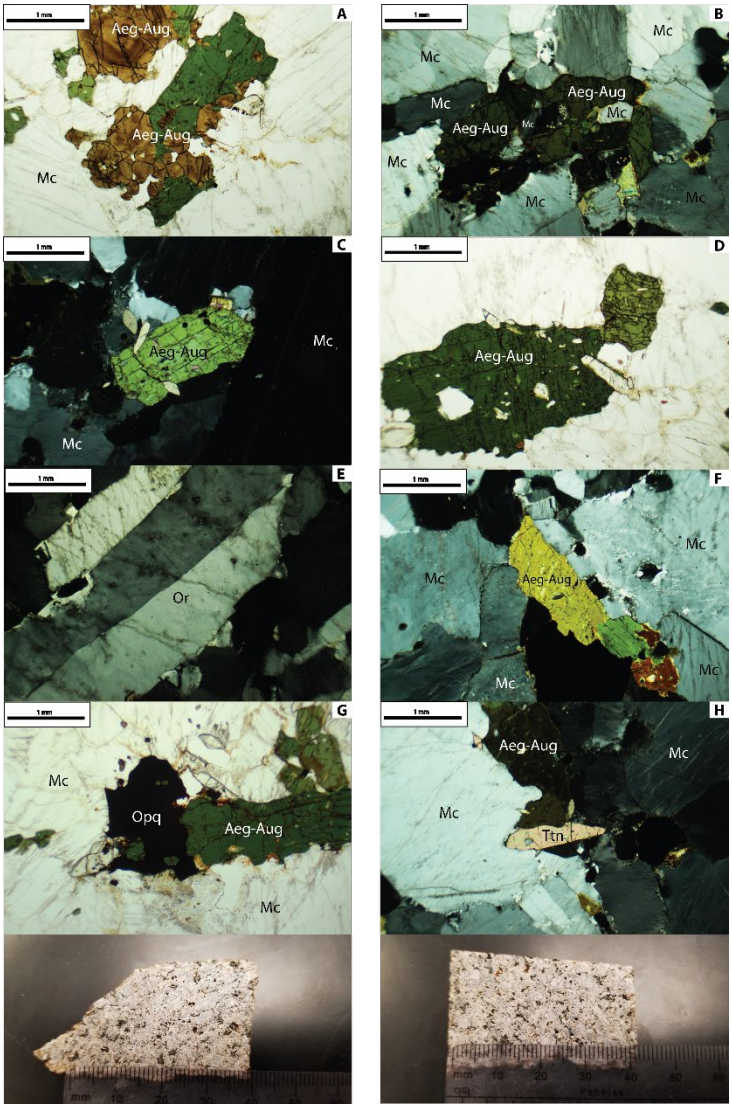

Figure 7: Microphotograph of nepheline syenite taken from a transmitted light microscope. Aeg-Aug, aegerine-augite; Mc, microcline; Or, orthoclase; Opq, opaque mineral; Ttn, titanite.

Carbonatite:

The carbonatite is found as a stock roughly in the center of the complex. Carbonatite dike swarms crosscut the pyroxenite, uncompahgrite, and ijolite from the north to the southeast (Figure 1). The carbonatite sample was collected just to the south of the main stock (Table 1).

The carbonatite is mostly a white-tan color with dark brown-red spots of oxidation. The rock contains fine to 5 mm carbonate crystals with veins and spots of oxidation. This rock was observed from two thin sections (AM-Iron Hill-Carb1 and 1M-Carb-2011) that are different from each other. 1M-Carb-2011 has muscovite and carbonates being phlogopitized. AM-Iron Hill-Carb1 has large euhedral crystals of carbonates (predominately ankerite (Erickson, 2014)). Orthoclase clusters ranging 0.3 to 3.25 mm, along with iron oxide minerals, are scattered over the carbonates and found in their interstitials. Trace amounts of sulfides occur in the large ankerite crystals or groundmass as opaques (Erickson, 2014). Iron oxide alteration after the ankerite forms rhombohedral patterns.

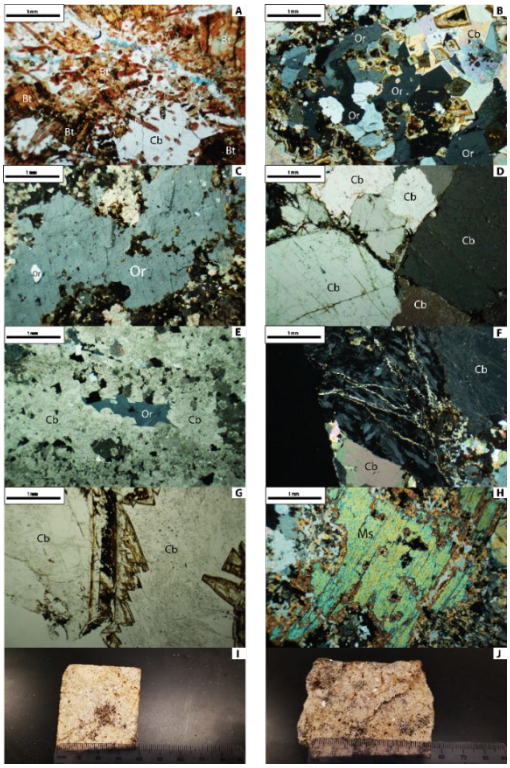

Figure 8: Microphotograph of nepheline syenite taken from a transmitted light microscope. Bt, biotite; Cb, carbonate minerals; Ms, muscovite; Or, orthoclase.

Isotopes

TABLE 3: THE ISOTOPIC Sr AND Nd VALUES OF THE POWDERHORN CARBONATITE COMPLEX ROCK SUITE

Sample Name	Rock Type	[Rb]*	[Sr]*	$Sr^{87}/Sr^{86}_{(m)}$	$Sr^{87}/Sr^{86}_{(i)}$	$\varepsilon Nd_{(i)}$
This Project						
AM-Iron Hill-Uncom-1	Uncompaghrite	11.2255	3907	0.703370± 0.000012	0.703298	N.D
AM-Iron Hill-Ijo-1	Ijolite	3.8976	1080.1	0.703723± 0.000011	0.703632	N.D
AM-Iron Hill-Pyro-4	Pyroxenite	5.8023	536.57	0.703511± 0.000010	0.703239	N.D
AM-Iron Hill-Carb-1	Carbonatite	0.28641	8065	0.703107± 0.000009	0.703106	N.D
Premo and Lowers (2013)						
	Pyroxenite	N.D	N.D	N.D	0.70343 ± 0.00010	N.D
	Combining pyroxenite, mix rock, and carbonatite values	N.D	N.D	N.D	0.7026-0.7038	+1.4-+3.1

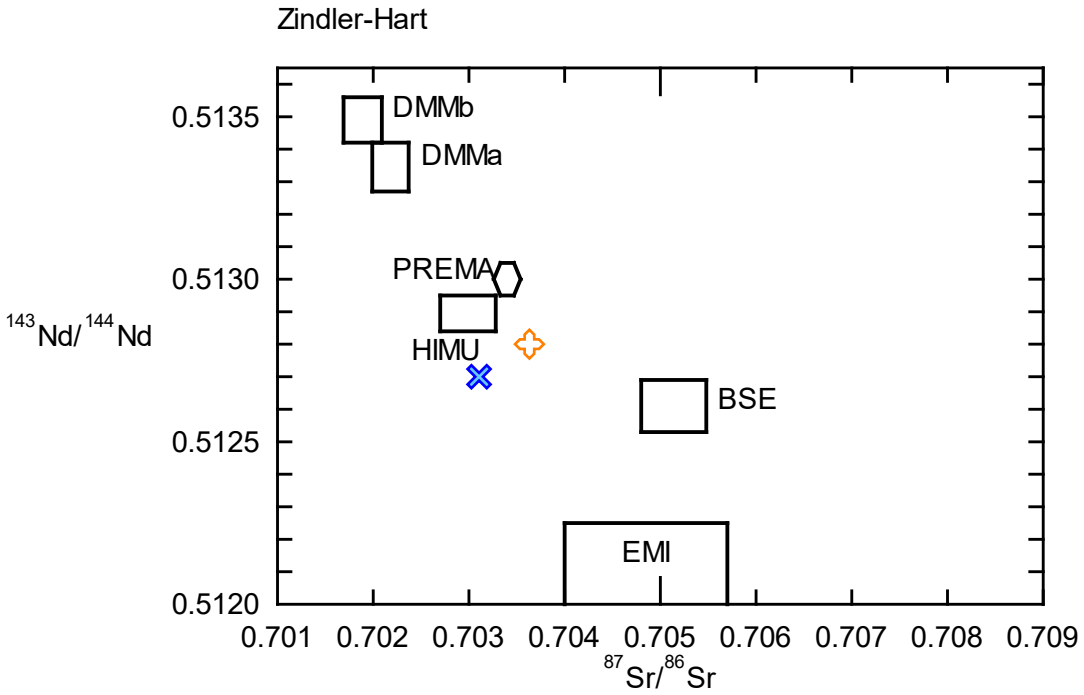

Figure 9: Comparing the Nd and Sr isotopes of pyroxenite and carbonatite to the heterogeneous mantle sources using Zindler and Hart (1986) Mantle Isotopic Diagram. An increase in Sr isotope means more enriched sources, and an increase in Nd isotope means more depleted source. Sr isotope data came from this project; Nd isotope is from Premo and Lowers (2013). The blue cross represents the pyroxenite, and the hollow yellow cross represents the carbonatite. These points plot near the HIMU and Prema reservoirs. The other boxes represents other mantle sources: DMM, depleted mantle; BSE, bulk silicate earth; and EM1

Nd and Sr Isotopic Data

Previous Sr/Nd isotope analysis at the Powderhorn Complex was done by Powell (1962) and Premo and Lowers (2013). Powell used Sr isotopes on all the rock types. While the pyroxenites have similar signatures to ours (0.7033), the signatures of the other rocks are higher (0.7060 to 0.7087). This difference is caused by Powell not using ratios that are correlated to the age of the complex. The other project, Premo and Lowers (2013) used Nd and Sr ratios that are time correlated similar to ours (~600 Ma). Since their time correlation and Sr values are similar to ours (Table 3), their Nd data will be incorporated with ours.

The Sr and Nd data and initial values for this project are set during the formation of the complex, approximately 600 Ma. For the Sr initial values, lowest value is from the carbonatite at 0.703106 and the highest values from the ijolite at 0.703632 (Table 3). Initial εNd by combining

the pyoxenite, carbonatite, and pyroxenite-nepheline syenite mixed rock ranges at 1.4-3.1. The values were plotted on Zindler-Hart (1996) plot. On this plot, the Powderhorn Carbonatite Complex samples plot near the HIMU field (Fig. 9).

Bulk-rock Geochemical Data

Major Elements

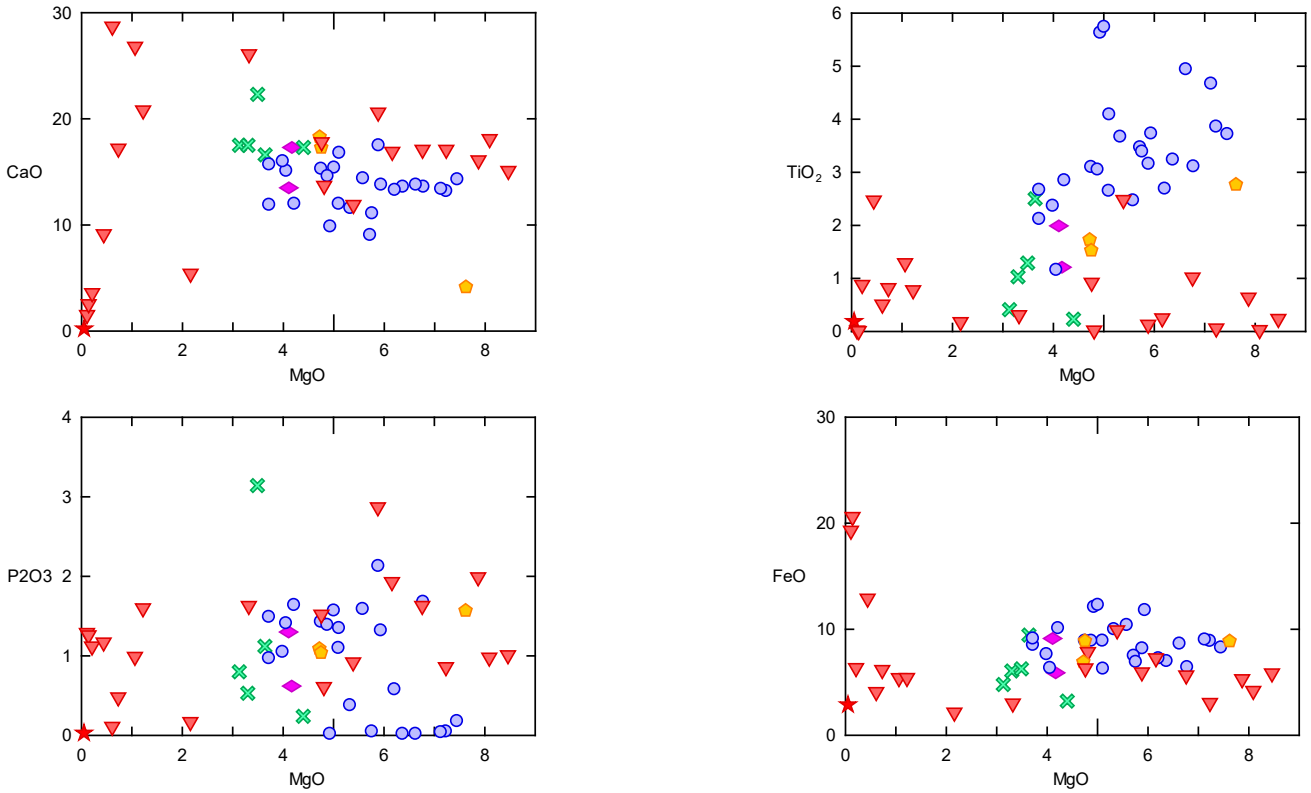

Figure 10: Bivariate plots of CaO, TiO_2, P_2O_5, FeO vs. MgO compared to pyroxenite (blue circles), ijolite (pink diamonds), uncompahgrite (green Xs), carbonatite (red triangles), pyroxenite-nepheline syenite mixed rock (golden pentagons), and nepheline syenite (red stars). Data from Van Goosen (2008).

Previous whole rock geochemistry was done by Van Goosen (2008), who collected 57 whole rocks samples throughout the complex, and analyzed their geochemistry. Since we did not

collect enough rocks to have concrete geochemical evidence, we combined our data with Van Goosen's. To view the entire whole rock geochemical analysis of this project, refer to Appendix A.

The pyroxenite plots show an increase in TiO_2 and P_2O_5 with increasing MgO. Both the uncompahgrite and ijolite show an increase in CaO, TiO_2, P_2O_5, FeO, and while the MgO relatively stays constant. The carbonatites does not follow a trend, and instead scatters. The pyroxenite-nepheline syenite mixed rock roughly follows the pyroxenite trend. All of the rock type data in the La/Lu plot are enriched in CaO and MgO, and depleted in La/Lu, except for a few scattered carbonatite points.

Trace Elements

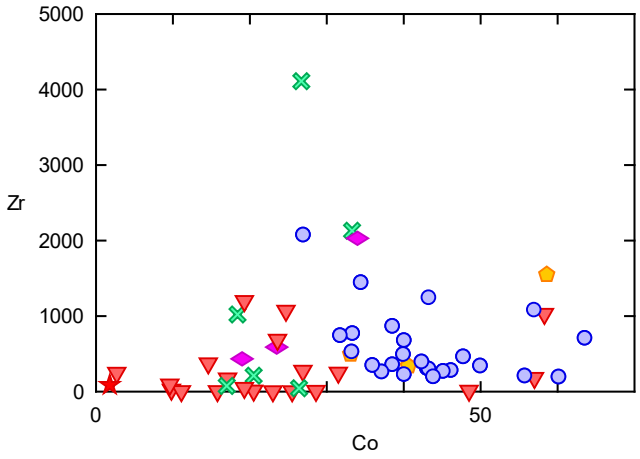

Figure 11: Bivariate plots of Zr vs. Co of pyroxenite (blue circles), ijolite (pink diamonds), uncompahgrite (green Xs), carbonatite (red triangles), pyroxenite-nepheline syenite mixed rock (golden pentagons), and nepheline syenite (red stars). From combination of Van Goosen (2008) and this project's data.

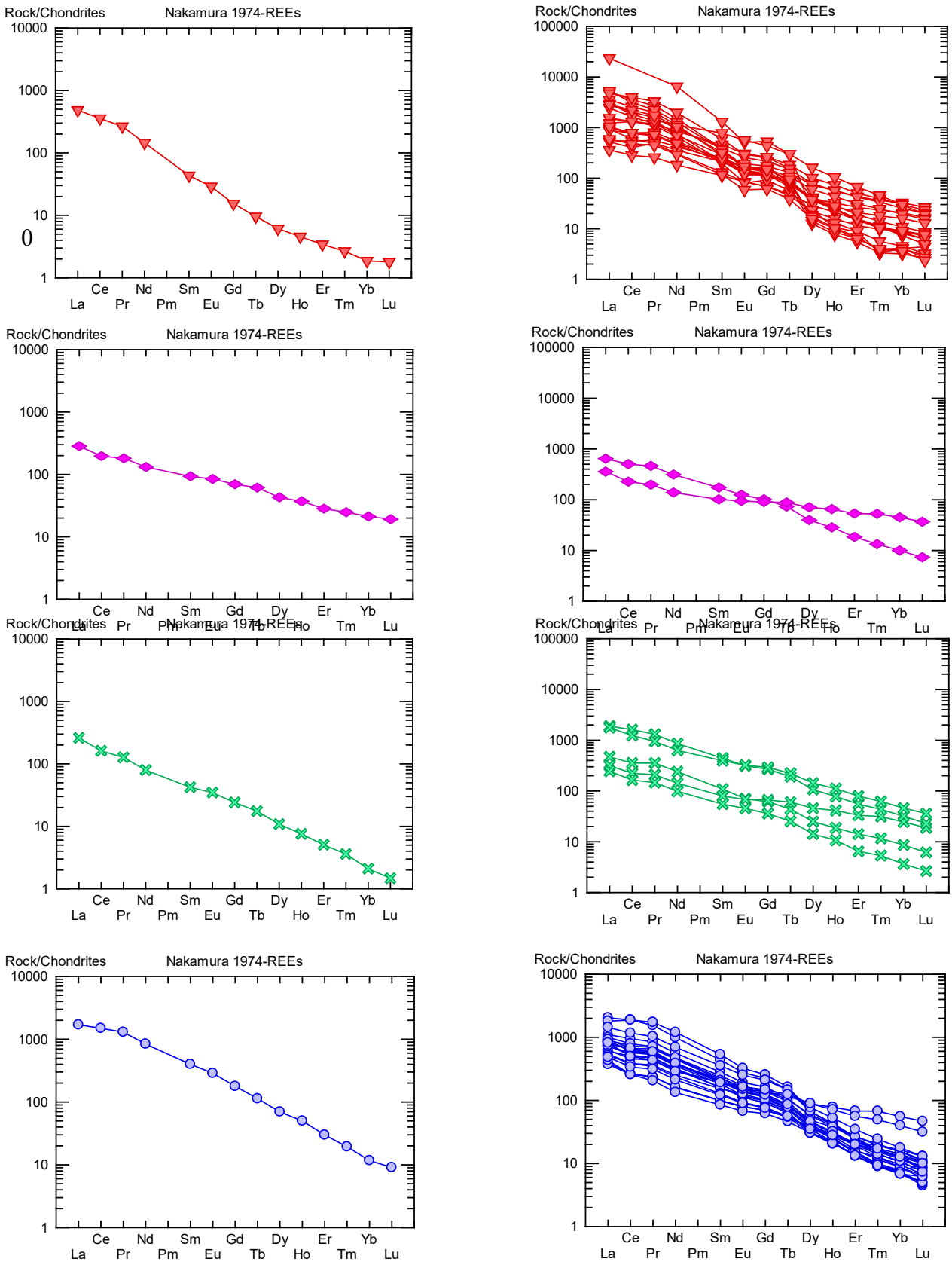

Figure 12: Chondrites-Normalized REE patterns of pyroxenite (blue circles), ijolite (pink diamonds), uncompahgrite (green Xs), and carbonatite (red triangle). The left plots are from this project, right plots are from Van Goosen (2008). Chondrite normalizing values from Nakamura (1974).

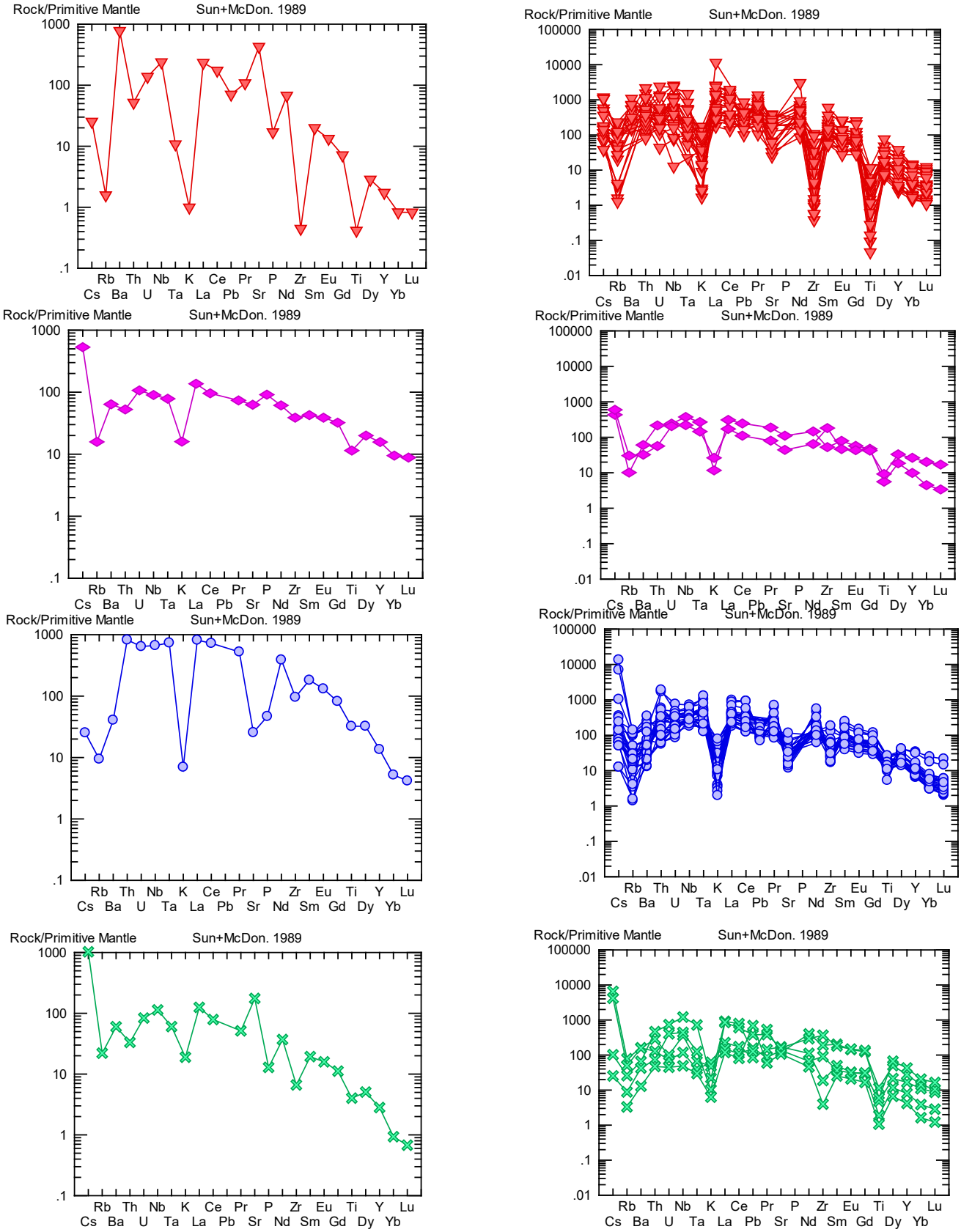

Figure 13: Primitive Mantle-Normalized trace elements patterns of pyroxenite (blue circles), ijolite (pink diamonds), uncompahgrite (green Xs), and carbonatite (red triangle). The left plots are from this project, right plots are from Van Goosen (2008). Chondrite normalizing values from Sun and McDonough (1989).

A bivariate plot was created for Zr and Co concentrations for each rock type (Fig. 11). The reason why these two trace elements were chosen because Zr is incompatible in ultramafic rocks while Co is compatible. The pyroxenite field contains the most Co and low to intermediate Zr. with a gradual increasing trend. The uncompahgrite and ijolite have intermediate Co, and low to high Zr. The carbonatite has mostly low Co and low to intermediate Zr. For chondrite values (Nakamura, 1974), all the rock types are enriched in LREEs, whereas the HREEs get less enriched and flattens out (Fig. 12). The rocks follow similar trends on primitive mantle-normalized plots (Sun and McDonough, 1989) (Fig. 12). Also in this normalization, all the rocks show depletion in Rb, K, P, Zr, and Ti and enrichment in Th, U, Nb, Ta, and Pb. The pyroxenite is the most enriched in light REEs along with Th, U, Nb, Ta, Zr, and Ti. The uncompahgrite has depletion of light REEs from La-Sm, Lu, and most enriched in Cs and Sr. The ijolite is also enriched in Cs, the heavy REEs, and the most normalized to chondrites, and primitive mantle values. Finally, the carbonatite depleted in Lu, Ta, and enriched in Ba, and Sr.

When the plots of this project were compared to the plots of Van Goosen (2008), they follow similar trends, but have a few differences in trace element depletion and enrichment. For the Sun and McDonald (1989) primitive mantle values, Van Goosen's data has the carbonatite as the most enriched in U, Nb, Ta, La, Ce, Nd, Pr, Sm, Eu, Gd, Dy and depleted in Nb (Fig. 12). The pyroxenite is the most enriched in Cs, Lu and the most depleted in Cs. The uncompahgrite and ijolite are more enriched in Zr. For the nepheline syenite, this rock is depleted in U, La, Ce, Pr, Nd, Dy, Y, Yb, Lu and enriched in K. The mixed rock almost follows the same pattern as the nepheline syenite with the exception from being slightly more enriched in most of the trace elements, and being enriched in Cs.

DISCUSSION

The similar yet slightly varied isotopic signatures, discrete fields of bivariate plots, unique mineralogy of each rock type, and enrichment of LREEs and HFSEs could indicate that these rocks were formed by the processes of crustal contamination, crystal fractionation, degree of partial melting, and minor heterogeneous source controlled by composition.

The whole-rock Sr and Nd isotope ratios are similar for all rock types in the Powderhorn Complex, but there is a noted variation in the Nd values. The Sr isotope ratios are between 0.703106 and 0.703632, whereas the Nd epsilon values range from +1.4 to +3.1 (Table 3) (Premo and Lowers, 2013). While Premo and Lowers (2013) stated that the low Nd values could indicate crustal contamination, there were no xenoliths/xenocrysts found in the thin section of the rock types or in the field. In addition to finding no xenoliths, it is impossible to characterize whether the heterogeneity of the source area for these rocks is controlled by metasomatism, ancient subducted material, or both. The other possible explanation, which involves minor variations in the composition of the magma source, is more likely, given the lack of evidence for contamination, and the narrow range of Sr isotope data. Overall, suite of rocks in the Powderhorn Complex have isotopic signatures similar to those of the HIMU (high $^{238}U/^{204}Pb$ source) and PREMA (prevalent mantle) fields of oceanic island basalts (Figure 9). HIMU sources are commonly believed to have formed from subduction of oceanic plates that were metasomatized (Rollinson, 1993; Dickin, 2005). PREMA either formed by the mixing of other mantle sources or is one the earlier mantles of the Earth (Dickin, 2005). The small deviation of Sr isotope data are more convincing of a similar source than the Nd, but the Nd data indicate something happened to that source area. One possibility is by metasomatism (Chun Li et al., 2018).

Nash (1972) speculated that the rocks of the complex originated from a carbonated nephelinite parent magma while Erickson (2014) inferred that the pyroxenite partially melted from a primitive mantle source. They both agree that this parent magma was controlled by crystal fractionation which yield the complex's silicate rocks, pyroxenite, uncompahgrite and ijolite. During the formation of the ijolite, the magma was enriched with CO_2 and H_2O from the previous fractionation process, causing the magma to split into a carbonate and silicate melt. This carbonate melt became the carbonatite, and the silicate became the nepheline syenite. Both Nash (1972) and Erickson (2014) used microprobe analysis on pyroxene from each rock type throughout the complex. Support for Erickson (2014)'s crystal fractionation hypothesis comes from the continuous trends in major elemental chemistry of the pyroxenes such as decreasing Ca/Na and Mg/Fe ratios as well as end-member composition (diopside to aegirine) as the rocks gets younger. We agree that these rocks originated from a primitive mantle source possibly through partial melting, but we disagree on that the silicate rocks were controlled by crystal fractionation of a common parent magma. In addition, although similar isotope ratios can indicate immiscibility (Bell, 1998), we did not collect isotope data for the nepheline syenite, and it is impossible to discuss the immiscibility story of the complex.

The whole-rock geochemical data (Appendix A.) of the rock types plot in distinct fields on various discriminant diagrams, and have slight differences in REE concentrations and trends. Erickson (2014) and Nash (1972) argued that the different rocks in the Powderhorn Complex were related by fractional crystallization of the pyroxenite magma. Microprobe data of pyroxene were used in both studies. Erickson (2014) used Nash (1972)'s major elements data of pyroxene from pyroxenite, uncompahgrite, ijolite, and nepheline syenite and plotted it on a diopside-hedenbergite-aegirine ternary plot. The plot infers that crystal fractionation occurred as younger

rocks are more aegirine rich and older rocks are more diopside rich. Erickson also measured decreasing Ca/Na and Mg/Fe ratio trends in the pyroxenes as well. Since fractionation will always occur within the genesis of an individual crystal, analyzes will support crystal fractionation. This is not a powerful technique to analyze the whole rock evolution. As shown by the whole rock geochemistry plots in this project, the rocks of Powderhorn are not related to a single magma, with the exception of the pyroxenite suite. On various X-Y plots, samples from the pyroxenite do define a somewhat linear trend indicating that this magma likely underwent continuous fractionation of a given mineral or minerals during emplacement and crystallization. The fields defined by data for the uncompahgrite and ijolite, however, are more difficult to interpret. The plots reveal that these rocks types were either derived from distinct magma compositions or there were extreme changes in mineral assemblages that fractionated relatively independent from each other. MgO vs CaO, FeO, TiO_2, and, P_2O_3 plots were made to see if the rock types are controlled by crystal fractionation. On the MgO bivariate plots (Fig. 10), each rock type plots in a discrete field. The carbonatite is mostly scattered on every bivariate plot and shows no trends. The uncompahgrite and ijolite both show relatively constant MgO and increasing CaO, FeO, TiO_2, and P_2O_3, indicating rapid composition change. The pyroxenite also show increasing P_2O_3, relatively constant CaO and FeO with increasing MgO, and a rough positive increasing trend on the TiO_2. This trend could possibly indicate crystal fractionation within this suite and possibly explain its unique mineralogical members. Zr vs. Co plot were also made to see if rocks were controlled by crystal fractionation (Fig. 11). With one axis being an incompatible element (Zr) and the other compatible (Co), if crystal fractionation occurred, then there should be a positive linear trend. Instead, each rock type forms discrete fields in a relative random pattern. The pyroxenite field contains the most Co and low to intermediate Zr with a gradual increasing trend. The uncompahgrite and ijolite has

intermediate Co, and low to high Zr. The carbonatite has mostly low Co and low to intermediate Zr. The presence of these unique discrete fields indicate that each rock was formed from an independent parent magma, and not through fractional crystallization of a common parent magma as previous sources stated by Nash (1972) and Erickson (2014).

Plots of REE data for the different rock types in the Powderhorn Complex reveal that all have elevated LREE with slight variations in HREE enrichment. The similar patterns reveals on these plots suggest a similar, but not homogeneous, magma source. The Nakamura (1974) REE plots (Fig. 12) shows that all the rock types follow a similar trend of being enriched in LREEs and gradually become more depleted the heavier the REE is until the end where it flattens out. The carbonatite, pyroxenite, and uncompahgrite are most enriched in LEEs with values more than 1000 times chondrite values, whereas the ijolite have between 100 and 1000 times chondritic values. When compared to the Sun and McDonough (1989) primitive mantle spider diagrams (Fig. 12), all the rocks are mostly enriched in some HFSE (high field strength elements) such Nb, U, LREEs, Th, and depleted in some such as Zr, Ti, and HREEs. These rocks are also depleted in main crustal LILE (large ion lithosphere elements) such as Rb, K, Sr, and Ba, but there is enrichment in Cs. The trace element plots show that these rocks these rocks originated from an enriched source rather than a depleted one. The enrichment could possibly be controlled by the source rock's compositional variation, partial melting, or through crustal contamination.

If the different rock types were related by crystal fractionation then this should be revealed on the geochemical plots. If related by fractionation, then on the MgO (Fig. 10) and Zr vs Co (Fig. 11) plots, there would less discrete fields and more linear trends from pyroxenite to ijolite. The pyroxenite has higher amount of LREEs than the ijolite. This would be reversed if crystal fractionation occurred. Since radiogenic isotopes do not fractionate by chemical processes

(Dickins, 2005), all the rock types controlled by crystal fractionation should have the same isotopic signatures, but they do not. Another evidence that fractionation was not responsible for the composition variation in the comples is that all of the rock types in the field have sharp contacts with each other, and there are no intermediate lithologies (with the one exception of the mixed rock of pyroxenite and nepheline syenite (Armbrustmacher, 1981)).

Another possible way that the Powderhorn rocks could have formed involves upper mantle or crustal contamination. According to Premo and Lowers (2013), the εNd of +1.4 to +3 indicates that there was crustal contamination during magmatic formation. In this project, there was no evidence of crustal contamination in all the rocks such as xenocrysts or xenoliths. The ijolite contains plagioclase and quartz veins and has the highest Sr isotope value at 0.703632. The presence of plagioclase and quartz veins could indicate contamination, but these minerals most likely formed in late stages of crystallization (plagioclase) or through post magmatic events (quartz) such as the Laramide Orogeny, and/or San Juan Volcanics event.

Another process that could explain the formation and variation in each rock type is different degrees of partial melting. Van Goosen (2009) stated that the complex was formed by the partial melting of carbonated peridotite. Different degrees of partial melting has been known to cause chemical composition changes in the magma (Rollinson, 1993) It also has been known that many alkaline silicate melts in mantle are formed from the discrete partial melting of an isotopically heterogeneous mantle and can release CO_2 fluids/melts, and cause metasomatism, and carbonatite melts (Bell, 1998; Hoernle et al., 2002).

The minor heterogeneity in isotopic and geochemical signatures of the rocks in Powderhorn could have formed in different zones of the source, and the mineralogy could be controlled by varying compositions. The HIMU signatures and low amounts of crustal elements

such as Rb and K indicate that these rocks originated in the lower mantle (Faure, 1986; Mittlefehldt, 1999; Winter, 2010). Previous seismic studies reveal that the lower mantle is heterogeneous (e.g. Hedlin et al., 1997; Niu and Kawakatsu, 1997; Castle and Creager, 1999; Deuss and Woodhouse, 2002). This is also supported by isotopic and trace element studies from oceanic basalts (e.g. Zindler and Hart, 1986; Hofmann, 1997). It is known that the 1000 kilometer lower mantle is chemically heterogeneous, based on tomographic mapping and density functions for temperature, perovskite, and iron variations (Van der Hilst and Karason, 1999). It is also known that HIMU sources are isotopically evolved subducted material such as oceanic crust, pelagic/terrigenous sediment, delaminated lower continental crust, suboceanic and subcontinental lithosphere (White and Hofmann, 1982; Zindler and Hart, 1986; Hofmann, 1997; Stracke et al., 2003; Tatsumi and Kogiso, 2003; Jackson et al., 2007).

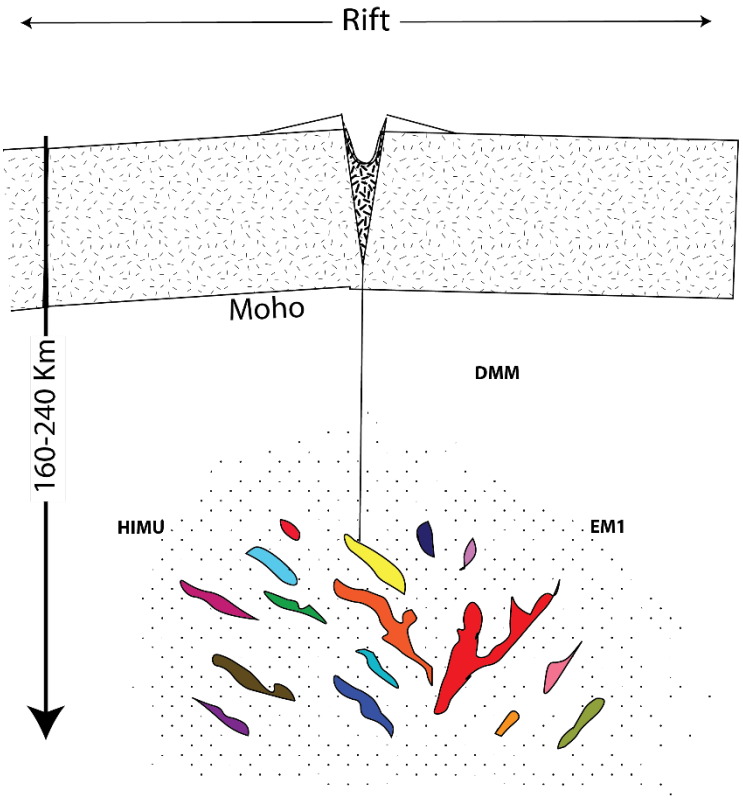

Figure 14: Overview cartoon on the formation of the Powderhorn complex. The varied colored magma represents heterogeneity in the source area with respect to different mantle sources. Stipples indicates metasomatism Modified from Ehrenberg (1979).

Conclusion

A viable model for the Powderhorn Complex rock types is that they were derived from a similar carbonated HIMU or PREMA mantle source with minor variation in the isotopic and compositional signatures (Fig. 14). The similar Sr signatures indicate a similar source, and the low Nd shows that something happened to the source area or magma, possibly crustal contamination or metasomatism. There is no evidence that crustal contamination of these magmas caused the isotopic variations due to the lack of xenoliths/xenocrysts. The lack of xenoliths/xenocrysts also makes it impossible to predict what the source area environment was like, such as whether metasomatism or if ancient subducted material were involved. Each rock type has a unique mineralogy and texture. This could be caused by individual parent magmas coming from different parts of a minor heterogeneous mantle source. The source could also have been further modified by different degrees of partial melting. The geochemistry also shows that each rock is consistent with the idea that different rock types formed from compositionally distinct magmas, as opposed to evolution via fractional crystallization. Evidence that disproves crystal fractionation includes unique discrete fields of each rock type on the geochemical plots, higher enrichment of LREEs in pyroxenite than ijolite, varied isotopes between each rock, and lack of intermediate lithologies in the field.

There is still more potential work that can help add to the Powderhorn Carbonatite Complex story. The nepheline syenite needs to have whole rock isotopic and geochemical studies, and be compared to the rest of the Powderhorn rock suite. According to Erickson (2014), a 3D-

surface model of the complex created from logging of drill cores can show the spatial relationship between the carbonatite and nepheline syenite to see if they were immiscible melts. Another study suggested by Erickson (2014) that needs explanation is how the pyroxenite unit followed its own magmatic evolution that is separate from the rest of the rock types. To truly see if there was contamination in the complex, Nd isotopes of individual crystals can be done to see if their isotopic ratios changes throughout the crystal.

REFERENCES

Armbrustmacher, T.J., 1981, The complex of alkaline rocks at Iron Hill, Powderhorn District, Gunnison County, Colorado: New Mexico Geological Society Guidebook, 32nd Field Conference, Western Slope Colorado.

Bell, K., 1998, Radiogenic isotope constraints on relationships between carbonatites and associated silicate rocks-a brief review: Journal of Petrology, v. 39, p. 1987-1996.

Berger, V.I., Singer, D.A., and Orris, G.J., 2009, Carbonatites of the world, explored deposits of Nb and REE—database and grade and tonnage models: U.S. Geological Survey Open-File Report 2009-1139, p. 17, and database [http://pubs.usgs.gov/of/2009/1139/].

Brey, G.P., Bulatov, V.K., Girnis, A.V., and Lahaye, Y., 2008, Experimental melting of carbonated peridotite at 6-10 GPa: Journal of Petrology v. 49, p. 797-821.

Castle, J.C., and Creager, K.C., 1999, A steeply dipping discontinuity in the lower mantle beneath Izu-Bonin: Journal of Geophysical Research, v. 104, p. 7279-7292.

Cappa, J., 1998, Alkalic igneous rocks of Colorado and their associated ore deposits: Colorado Geological Survey, Resource Series 35, p. 61-68.

Chun Li, X.., Fu Zhou, M., Heng Yang, Y., Fu Zhao, X., and Feng Gao, J., 2018, Disturbance of the Sm-Nd isotopic system by metasomatic alteration: A case study of fluorapatite from the Sin Quyen Cu-LREE-Au deposit, Vietnam: American Mineralogist, v. 103, p.1487-1496.

Deuss, A., and Woodhouse, J.H., 2002, A systematic search for mantle discontinuities using SS-precursors: Geophysical Research Letters, v. 29 doi: 10.1029/2002GL014768.

Dickin, A. P., 2005, Radiogenic Isotope Geology (2nd ed.): Cambridge University Press, p. 151 and 157.

Ehrenberg, S. N., 2013, Garnetiferous Ultramafic Inclusions in Minette from the Navajo Volcanic Field. In The Mantle Sample: Inclusion in Kimberlites and Other Volcanics (eds F. Boyd and H. O. Meyer). doi:10.1029/SP016p0330.

Erickson, J., 2014, Rare-earth element mineralization and formation of Iron Hill carbonatite complex, Gunnison County, Colorado, USA (Masters Thesis): Golden, Colorado School of Mines.

Farmer G.L., Broxton, D.E., Warren, R.G., and Pickthorn, W., 1991, Nd, Sr, and O isotopic variations in metaluminous ash-flow tuffs and related volcanic rocks at the Timber Mountain/Oasis Valley Caldera Complex, SW Nevada: implications for the origin and evolution of large-volume silicic magma bodies: Contributions to Mineralogy and Petrology, v. 109, p. 53-68.

Faure, G., 1986, Principles of Isotope Geology: John Wiley and Sons, p. 217-234.

Gittins, J., 1989 , The origin and evolution of carbonatite magmas , in Bell , K. , ed. , Carbonatites : Genesis and evolution: London , Unwin Hyman , p. 580-600.

Gittins, J., Jand ago, B.C., 1998, Differentiation of natrocarbonatite magma at Oldoinyo Lengai volcano, Tanzania: Mineralogical Magazine, v. 62, p. 759-768.

Goetz, L. K., and Dickerson, P. W., 1985, A Paleozoic transform margin in Arizona, New Mexico, west Texas and northern Mexico; in Dickerson, P. W., and Muehlberger, W. R. (eds.), Structure and tectonics of TransPecos Texas: West Texas Geological Society, Field conference guidebook, Publication 8581, pp. 173–184.

Gonzales, D,G., and Lake, E,T., 2016, Geochemical constraints on mantle-melt sources for Oligocene to Pleistocene mafic rocks in the Four Corners region, USA: Geosphere, v.13, no.1, doi:10.1130/GES01314.1.

Harmer, R. E., and Gittins, J., 1997, The origin of dolomitic carbonatites: field and experimental constraints: Journal of African Earth Sciences, v. 25, p. 5-28.

Harmer, R. E., and Gittins, J., 1998, The case for primary, mantle-derived carbonatite magma: Journal of Petrology, v. 39, p. 1895-1903.

Halama, R., Vennemann, T., Siebel, W., and Markl, G., 2005, Gronnedal-Ika carbonatite syenite complex, South Greenland: carbonatite formation by liquid immiscibility: Journal of Petrology v. 46, p. 191-217.

Hedlin, M.A.H., Shearer, P.M., and Earle, P.S., 1997, Seismic evidence for small-scale heterogeneity throughout the Earth's mantle: Nature, v. 387, p. 145-150

Hedlund. D.C., and Olson. J.C., 1981, Precambrian geology along parts of the Gunnison uplift of southwestern Colorado: New Mexico Geological Society 32nd Annual Fall Field

Conference Guidebook, pp. 267-272.

Hoernle, K.A., Tilton, G.R., Le Bas, M.J., Duggen, S., and Garbe-Schonberg, D., (2002) Geochemistry of oceanic carbonatites compared with continental carbonatites: mantle recycling of oceanic crustal carbonate: Contributions to Mineralogy and Petrology, v. 142, p. 520–542.

Hofmann, A.W., 1997, Mantle geochemistry: The message from oceanic volcanism: Nature, v. 385, p. 219–229, doi:10.1038/ 385219a0.

Jackson, M. G., Kurz, M. D., Hart S. R., and Workman R. K., 2007, New Samoan lavas from Ofu Island reveal a hemispherically heterogeneous high He-3/He-4 mantle, Earth and Planetary Science Letters, v. 264, p. 360–374, doi:10.1016/j.epsl. 2007.09.023.

Jones, A. P., Genge, M., and Carmody, L., 2013, Carbonate melts and carbonatites: Reviews in Mineralogy & Geochemistry, v. 75, p. 289-322.

Koster Van Groos, A.F., and Wyllie, P.J., 1963, Experimental data bearing on the role of liquid immiscibility in the genesis of carbonatites: Nature, v. 199, p. 801-802.

Kjarsgaard, B., and Hamilton, D.L., 1989, The genesis of carbonatite by immiscibility, Carbonatites: Genesis and Evolution: London: Unwin Hyman, p. 388-404.

Larsen, E. S., Jr., 1942, Alkalic rocks of Iron Hill, Gunnison County, Colorado: U.S. Geological Survey Professional Paper 197A, p. 1-64.

Le Maitre, R.W., ed., 2002, Igneous rocks—A classification and glossary of terms: Cambridge, United Kingdom, Cambridge University Press, p. 236.

Li, Z.X., et al, 2008, Assembly, configuration, and break-up history of Rodinia: A synthesis: Precambrian Research, v.160, p. 179-210.

McMillian, N.J., and McLemore, V.T., 2004, Cambrian–Ordovician magmatism and extension in New Mexico and Colorado: New Mexico Bureau of Geology and Mineral Resources, Bulletin 160.

Mittlefehldt, D.M., 1999, Potassium: From Encyclopedia of Geochemistry (Encyclopedia of Earth Sciences Series), Ed. Marshall, Clare P. & Fairbridge, Rhodes W. Springer. 522.

Nakamura, N., 1974, Determination of REE, Ba, Fe, Mg, Na and K in carbonaceous and ordinary chondrites: Geochimica et Cosmochimica Acta, v. 38, p.757-775.

Nash, W.P., 1972, Mineralogy and petrology of the Iron Hill carbonatite complex, Colorado: Geological Society of America Bulletin, v. 83, p. 1361-1382.

Niu, F., and Kawakatsu, H., 1997, Depth variation of the mid-mantle seismic discontinuity: Geophysical Research Letters, v. 24, p. 429-432.

Olson, J.C., Marvin, R.F., Parker, R.L., and Mehnert, H.H., 1977, Age and tectonic setting of lower Paleozoic alkalic and mafic rocks, carbonatites, and thorium veins in south-central Colorado: U.S. Geological Survey Journal of Research, v. 5, p. 673-687.

Olson, J.C., and Hedlund, D., 1981, Alkalic Rocks and Resources of Thorium and Associated Elements in the Powderhorn District, Gunnison County, Colorado: Geological Survey Professional Paper 1049-C, p. 1-34.

Powell, J.L., 1962, The strontium isotopic composition and origin of carbonatites (PhD: Cambridge, Massachusetts Institute of Technology.

Premo, W. R., and Lowers, H. A., 2013, Age and Origin of Pyroxenites from the Iron Hill Carbonatite Complex, Gunnison, Colorado: Evidence from Pb-Sr-Nd Isotopes: Rocky Mountain Section of the Geological Society of America and Associated Societies Abstracts with Programs, v. 45, p. 12.

Rollinson. H., 1993, Using geochemical data: evaluation, presentation, interpretation: Longman Scientific and technical, p. 249-265.

Stracke, A., Bizimis, M., and Salters V. J. M., 2003, Recycling oceanic crust: Quantitative constraints: Geochemistry, Geophysics, Geosystems, v. 4, p. 8003, doi:10.1029/2001GC000223.

Sun S., and McDonough W. F., 1989, Chemical and isotopic systematics of oceanic basalts: implications for mantle composition and process: Magmatism in Ocean Basins, Geological Society Special Publication, v. 42, p. 313-345.

Tatsumi, Y., and Kogiso, T., 2003, The subduction factory: Its role in the evolution of the Earth's crust and mantle, in IntraOceanic Subduction Systems, edited by R. Larter and P. T. Leat, Geological Society Special Publication, v. 219, p. 55 –80

Temple, A. K. and Grogan, R. M., 1965, Carbonatite and related alkalic rocks at Powderhorn, Colorado: Economic Geology, v. 60, p. 672-692.

Van Gosen, B.S., 2008, Geochemistry of rock samples collected from the Iron Hill carbonatite complex, Gunnison County, Colorado: United States Geological Survey, Open-File Report 2008-1119, 1-27 p.

Van Gosen, B., 2009, The Iron Hill (Powderhorn) carbonatite complex, Gunnison County, Colorado-a potential source of several uncommon mineral resources: United States Geological Survey, Open File Report 2009-1005, 1-29 p.

Van der Hilst, R.D., and Karason, H., 1999, Compositional heterogeneity in the bottom 1000 kilometers of Earth's mantle: toward a hybrid convection model: Science, v. 283, p. 1885-1887.

White, W. M., and Hofmann, A. W., 1982, Sr and Nd isotope geochemistry of oceanic basalts and mantle evolution: Nature, v. 296(5860), p. 821–825, doi:10.1038/296821a0.

Winter, J.D., 2010, Principles of Igneous and Metamorphic Petrology: Pearson Education, Inc, p. 397-420.

Wyllie, P. J., and Lee, W. J., 1998, Model system controls on conditions for formation of magnesiocarbonatite and calciocarbonatite magmas from the mantle: Journal of Petrology, v. 39, p. 1885-1893.

Wyllie, P. J., and Huang, W. L., 1975, Peridotite, kimberlite, and carbonatite explained in the system CaO-MgO-SiO2-CO2: Geology, v. 3, p. 621-624.

Zindler, A., and Hart, S., 1986, Chemical geodynamics: Annual Review of Earth and Planetary Sciences, v. 14, p. 493-571.

APPENDIX

APPENDIX A…: THE GEOCHEMISTRY OF THE ROCK TYPES AT POWDERHORN

Sample Rock Type	AM-IH-CARB-092118 Carbonatite	AM-IH-UNCOM-092118 Uncompaghrite	AM-IH-IJO-092118 Ijolite	AM-IH-PX-092118 Pyroxenite
SiO2	**2.17**	**39.17**	**39.79**	**30.24**
TiO2	0.09	0.869	2.475	6.995
Al2O3	0.15	7.82	10.06	6.28
Fe2O3	8.21	5.02	4.89	15.91
FeO	1.3	0.8	4.5	8.4
MnO	1.177	0.143	0.275	0.234
MgO	14.82	7.44	5.95	9.27
CaO	27.85	30.97	22.2	20.01
Na2O	0.04	0.56	2.29	0.34
K2O	0.03	0.57	0.48	0.21
P2O5	0.37	0.28	1.98	1.02
LOI	40.3	6.11	4.6	-0.23
LOI2	40.45	6.2	5.11	0.71
Total	96.65	99.83	100	99.62
Total 2	96.65	99.83	100	99.62
Sc	12	< 1	9	20
Be	4	16	4	2
V	48	45	383	307
Cr	40	< 20	< 20	480
Co	23	17	19	57
Ni	110	< 20	< 20	40

Cu	50	< 10	20	60
Zn	340	280	90	160
Ga	4	24	12	34
Ge	2.2	0.5	1.7	2.4
As	100	< 5	< 5	< 5
Rb	1	14	10	6
Sr	9002	3698	1320	540
Y	7.9	12.8	71.3	61.7
Zr	5	74	433	1076
Nb	170	80.9	64	476
Mo	5	< 2	5	< 2
Ag	0.6	0.5	2.9	7.4
In	0.2	< 0.1	0.2	0.2
Sn	< 1	1	4	6
Sb	10.3	0.3	< 0.2	< 0.2
Cs	0.2	8.1	4.2	0.2
Ba	5432	419	444	284
La	160	85.9	93.8	561
Ce	309	140	170	1290
Pr	29.8	14.2	20.3	145
Nd	91.5	50.1	82.7	528
Sm	8.83	8.58	18.9	81
Eu	2.23	2.67	6.51	22.1
Gd	4.25	6.65	19.2	49
Tb	0.45	0.82	2.88	5.32
Dy	2.1	3.72	14.7	23.9
Ho	0.32	0.53	2.6	3.5
Er	0.77	1.14	6.37	6.72
Tm	0.08	0.108	0.746	0.582
Yb	0.41	0.46	4.67	2.57
Lu	0.061	0.05	0.652	0.309
Hf	0.2	1.6	7.9	20.7
Ta	0.44	2.46	3.19	30
W	18.6	< 0.5	3	< 0.5
Tl	1.36	0.09	< 0.05	< 0.05
Pb	5	< 5	< 5	< 5
Bi	< 0.1	< 0.1	< 0.1	< 0.1
Th	4.41	2.82	4.47	70.1
U	2.89	1.75	2.24	13.5

Major Elements are measured in percentages relative to whole rock composition
Trace Elements are measured in parts per million

Values <1 were lower than the detection limit